Journal of Engineering Innovations & Technology (2024)

Journal of Engineering Innovations & Technology

journal homepage: www.journal-eit.online

Research article

Sliding mode active disturbance rejection control for manipulator considering actuator saturation

Dongyu Tian[1*]

1.School of Electronics and Information, Xi'an Polytechnic University, China

*Corresponding author

ABSTRACT

Considering the issue of low control accuracy in joint trajectory tracking control for manipulator systems with actuator saturation due to external disturbances, modelling inaccuracies, and joint friction, a sliding mode active disturbance rejection control approach was proposed. An improved extended state observer is employed to observe and estimate the lumped disturbances affecting the system, providing feedback compensation. A variable gain reaching law is devised, coupled with a fast non-singular terminal sliding mode to design the system control law, which mitigates chattering inherent and ensuring precision control. Additionally, a novel output error compensation-based anti-windup scheme is introduced to compensate for the detrimental impacts caused by actuator saturation. Simulation results collectively demonstrate that the proposed tracking control algorithm exhibits better control performance and robustness against disturbances.

Key words: robotic manipulator；trajectory tracking；active disturbance rejection control；sliding mode control；actuator saturation

0 Introduction

The mechanical arm is widely used in the production and detection fields because of its flexibility and high precision[1,2]. In a practical environment, the robotic arm is subject to model uncertainty, external disturbances, and a saturation phenomenon due to the physical characteristics of the device and its structural limitations[3,4]This leads to the deviation of system control accuracy, the reduction of system stability, and the failure to complete normal operations, which makes the research of trajectory tracking control strategy of great theoretical research significance and practical application value[5,6].

For the saturation problem, scholars often design and introduce the saturation compensation system to ensure the control performance of the system[7-9]. The traditional sliding mode control can only guarantee the gradual convergence of the system state, cannot guarantee the system state error converges to zero in finite time, and requires the disturbance, which greatly limits its application in actual industrial production. Fast non-singular terminal slide mode (fast non-singular terminal sliding mode, FNTSM)[10]The emergence overcomes the strange problem of terminal sliding mode and fast terminal sliding mode control input, and ensures the characteristics of finite time convergence, realizes the high precision trajectory tracking in finite time, but still has the problem of vibration, leading to the decline of system performance, and even aggravate equipment wear. This paper combines the idea of self-immunity control[11], a sliding-mode self-immunity control algorithm was designed.

1 Model description

1.1 Dynamic Model of Robotic Arm

According to Lagrange's theorem, considering robotic arms with n joints, whose kinetic equations can be described as[6]：

$$\boldsymbol{M}(\boldsymbol{q})\ddot{\boldsymbol{q}}+\boldsymbol{C}(\boldsymbol{q},\dot{\boldsymbol{q}})\dot{\boldsymbol{q}}+\boldsymbol{G}(\boldsymbol{q})=\boldsymbol{\tau}+\boldsymbol{\tau}_{\mathrm{d}}\,(1)$$

$\boldsymbol{q},\dot{\boldsymbol{q}},\ddot{\boldsymbol{q}}\in\mathbf{R}^n$ The manipulator joint angular position vector, angular velocity vector and angular acceleration vector respectively; is the inertia matrix; represents the centrifugal force and Coriz force matrix; is the gravity term; is the system control input; is the external interference. $\boldsymbol{M}(\boldsymbol{q})\in\mathbf{R}^{n\times n}$ $\boldsymbol{C}(\boldsymbol{q},\dot{\boldsymbol{q}})\in\mathbf{R}^{n\times n}$ $\boldsymbol{G}(\boldsymbol{q})\in\mathbf{R}^n$ $\boldsymbol{\tau}\in\mathbf{R}^n$ $\boldsymbol{\tau}_{\mathrm{d}}\in\mathbf{R}^n$

Usually in the actual control process, the dynamic model of the mechanical arm is imprecise, so its model parameters are assumed as follows:

$$\begin{cases}\boldsymbol{M}(\boldsymbol{q})=\boldsymbol{M}_0(\boldsymbol{q})+\eta\boldsymbol{M}(\boldsymbol{q})\\ \boldsymbol{C}(\boldsymbol{q},\dot{\boldsymbol{q}})=\boldsymbol{C}_0(\boldsymbol{q},\dot{\boldsymbol{q}})+\eta\boldsymbol{C}(\boldsymbol{q},\dot{\boldsymbol{q}})\\ \boldsymbol{G}(\boldsymbol{q})=\boldsymbol{G}_0(\boldsymbol{q})+\eta\boldsymbol{G}(\boldsymbol{q})\end{cases}(2)$$

$\boldsymbol{M}_0(\boldsymbol{q})$ $\boldsymbol{C}_0(\boldsymbol{q},\dot{\boldsymbol{q}})$ $\boldsymbol{G}_0(\boldsymbol{q})$ $\eta\boldsymbol{M}(\boldsymbol{q})$ $\eta\boldsymbol{C}(\boldsymbol{q},\dot{\boldsymbol{q}})$ $\eta\boldsymbol{G}(\boldsymbol{q})$ Where:, and is nominal;, and is the parameter difference between nominal and actual values.

Considering the safety problems and physical structure limitations of mechanical arms in practical applications, the saturation nonlinear characteristics often exist in the system, which can be described as:

$$\operatorname{sat}(u_i)=\begin{cases}u_{\max}, & u_i\ge u_{i\max}\\ u_i, & u_{i\min}<u_i<u_{i\max}\\ u_{\min}, & u_i\le u_{i\min}\end{cases}(3)$$

$i=1,2,\ldots,n$ u_i $u_{i\max}$ $u_{i\min}$ Where:; is the control law on the i th joint; and are the maximum and minimum values of the control input moment on the i th joint, respectively.

At this point, the kinetic model of the robotic arm can be expressed as:

$$\boldsymbol{M}_0(\boldsymbol{q})\ddot{\boldsymbol{q}}+\boldsymbol{C}_0(\boldsymbol{q},\dot{\boldsymbol{q}})\dot{\boldsymbol{q}}+\boldsymbol{G}_0(\boldsymbol{q})=\mathrm{sat}(\boldsymbol{u})+\boldsymbol{D} \quad (4)$$

$\boldsymbol{D}=\boldsymbol{\tau}_{\mathrm{d}}-\eta\boldsymbol{M}(\boldsymbol{q})\ddot{\boldsymbol{q}}-\eta\boldsymbol{C}(\boldsymbol{q},\dot{\boldsymbol{q}})\dot{\boldsymbol{q}}-\eta\boldsymbol{G}(\boldsymbol{q})$ Where: it is the total disturbance term of the system.

$\boldsymbol{x}=[\boldsymbol{x}_1 \;\; \boldsymbol{x}_2]^{\mathrm{T}}$ $\boldsymbol{x}_1=\boldsymbol{q}$ $\boldsymbol{x}_2=\dot{\boldsymbol{q}}$ Define a state variable, and then establish the following state equation according to equation (4):

$$\begin{cases}\dot{\boldsymbol{x}}_1=\boldsymbol{x}_2\\ \dot{\boldsymbol{x}}_2=\boldsymbol{M}_0^{-1}(\boldsymbol{x}_1)\mathrm{sat}(\boldsymbol{u})+\boldsymbol{P}(\boldsymbol{x})+\boldsymbol{F}\end{cases} \quad (5)$$

In formula: $\boldsymbol{P}(\boldsymbol{x})=-\boldsymbol{M}_0^{-1}(\boldsymbol{x}_1)\left(\boldsymbol{C}_0(\boldsymbol{x}_1,\boldsymbol{x}_2)\boldsymbol{x}_2+\boldsymbol{G}_0(\boldsymbol{x}_1)\right)$; 。 $\boldsymbol{F}=\boldsymbol{M}_0^{-1}(\boldsymbol{x}_1)\boldsymbol{D}$

2 Design of Sliding Mode Control with Disturbance Observer

For the mechanical arm dynamic system shown in formula (4), the design process of the proposed slip mode self-immunity control is given based on the ADRC idea and the stability theory of Lyapunov, and the structure of the control system is shown in Figure 1.

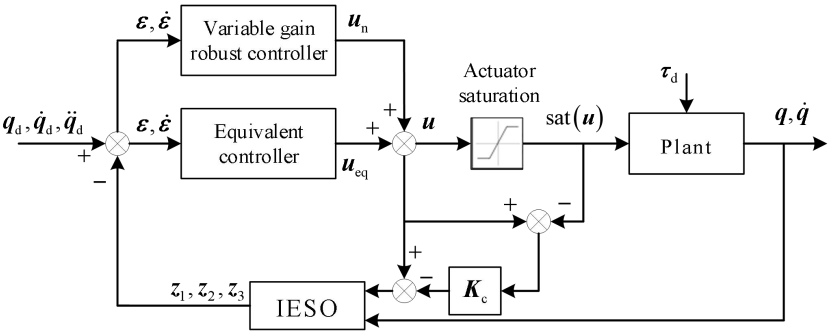

Fig 1 Control system structure block diagram

2.1 Design of Extended State Observer

As the core part of the self-resistant disturbance control framework, extended state observer (ESO) can observe the system state, estimate the system disturbance, and make feedback compensation. This paper introduces a new nonlinear function combined with self-immunity control theory to improve the expansion state observer (improved extended state observer, IESO):

$$\begin{cases} \boldsymbol{\varepsilon} = \boldsymbol{z}_1 - \boldsymbol{y} \\ \dot{\boldsymbol{z}}_1 = \boldsymbol{z}_2 - \beta_{01}\boldsymbol{\varepsilon} \\ \dot{\boldsymbol{z}}_2 = \boldsymbol{z}_3 - \beta_{02}\mathrm{ifal}(\boldsymbol{\varepsilon},\alpha_1,\mu) + b\boldsymbol{u} \\ \dot{\boldsymbol{z}}_3 = -\beta_{03}\mathrm{ifal}(\boldsymbol{\varepsilon},\alpha_2,\mu) \end{cases} \quad (6)$$

$\boldsymbol{\varepsilon}$ $\boldsymbol{y}$ $\boldsymbol{z}_1$ $\boldsymbol{z}_2$ $\boldsymbol{z}_3$ $\beta_{01},\beta_{02},\beta_{03}$ α_1,α_2,μ $\mathrm{fal}(\cdot)$ $\mathrm{ifal}(\cdot)$ Where: is the observation error; is the system output; is the output observation; is the differential observation; is the parameter affecting the observation effect; is the adjustable parameter; b is the controller gain. Compared with traditional mode, it is smoother and more continuous, and combined with sliding mode control is more conducive to reduce vibration, which can be described as:

$$\mathrm{ifal}(\varepsilon,\alpha,\mu) = \begin{cases} |\varepsilon|^{\alpha}\,\mathrm{sign}(\varepsilon), & |\varepsilon| > \mu \\ \kappa_1\varepsilon + \kappa_2\tan\varepsilon, & |\varepsilon| \le \mu \end{cases} \quad (7)$$

In formula: $\kappa_1 = \frac{\left(\sec^2\mu - \alpha\right)\mu^{\alpha-1}}{\tan^2\mu}$; 。$\kappa_2 = \frac{\left(\alpha-1\right)\mu^{\alpha-1}}{\tan^2\mu}$ According to the system (5), the total disturbance acting on the system is expanded into a new state variable, and the representation differential value is defined, then the state space equation of the system is expressed as: $\boldsymbol{x}_3 = \boldsymbol{P}(\boldsymbol{x}) + \boldsymbol{F}\ \omega(t)\ \boldsymbol{x}_3$

$$\begin{cases} \dot{\boldsymbol{x}}_1 = \boldsymbol{x}_2 \\ \dot{\boldsymbol{x}}_2 = \boldsymbol{M}_0^{-1}(\boldsymbol{q})\mathrm{sat}(\boldsymbol{u}) + \boldsymbol{x}_3 \\ \dot{\boldsymbol{x}}_3 = \omega(t) \\ \boldsymbol{y} = \boldsymbol{x}_1 \end{cases} (8)$$

2.2 Design of Sliding Mode Controller

FNTSM converges the state to zero in finite time by designing the sliding mode surface into a nonlinear superplane. To to the vibration problem, a sliding pattern is designed. The total disturbance of the system is estimated by IESO and input to the control end for feedback compensation, residual due to the uncertainty of the disturbance. After designing appropriate sliding mode control law, the system control error can close to 0.

$\boldsymbol{q}_\mathrm{d}, \dot{\boldsymbol{q}}_\mathrm{d}, \ddot{\boldsymbol{q}}_\mathrm{d}$ Defined as the joint angle, angular velocity and angular acceleration expectation signal respectively, the joint tracking error can be expressed as:

$$\begin{cases} \boldsymbol{\varepsilon} = \boldsymbol{q} - \boldsymbol{q}_\mathrm{d} \\ \dot{\boldsymbol{\varepsilon}} = \dot{\boldsymbol{q}} - \dot{\boldsymbol{q}}_\mathrm{d} \\ \ddot{\boldsymbol{\varepsilon}} = \ddot{\boldsymbol{q}} - \ddot{\boldsymbol{q}}_\mathrm{d} \end{cases} (9)$$

Design such as sliding surface:

$$\boldsymbol{s} = \dot{\boldsymbol{\varepsilon}} + \boldsymbol{K}_1\boldsymbol{\varepsilon} + \boldsymbol{K}_2\mathrm{sig}^r\left(\boldsymbol{\varepsilon}\right) (10)$$

$\mathrm{sig}^r(\cdot) = |\cdot|^r \mathrm{sign}(\cdot)$ $\boldsymbol{K}_1$ $\boldsymbol{K}_2$ In: define;, for the normal number diagonal matrix;.$1 < r < 2$

For equation (10):

$$\dot{\boldsymbol{s}}=\ddot{\boldsymbol{\varepsilon}}+\boldsymbol{K}_1\dot{\boldsymbol{\varepsilon}}+\boldsymbol{K}_2\Lambda|\boldsymbol{\varepsilon}|^{r-1}\dot{\boldsymbol{\varepsilon}}\,(11)$$

By formula (8) and formula (9), the above equation may be further expressed as:

$$\begin{aligned}\dot{\boldsymbol{s}}&=\dot{\boldsymbol{x}}_2-\ddot{\boldsymbol{q}}_{\mathrm{d}}+\boldsymbol{K}_1\dot{\boldsymbol{\varepsilon}}+\boldsymbol{K}_2r|\boldsymbol{\varepsilon}|^{r-1}\dot{\boldsymbol{\varepsilon}}\\&=\boldsymbol{M}_0^{-1}(\boldsymbol{q})\mathrm{sat}(\boldsymbol{u})+\boldsymbol{x}_3-\ddot{\boldsymbol{q}}_{\mathrm{d}}\quad(12)\\&\quad+\boldsymbol{K}_1\dot{\boldsymbol{\varepsilon}}+\boldsymbol{K}_2r|\boldsymbol{\varepsilon}|^{r-1}\dot{\boldsymbol{\varepsilon}}\end{aligned}$$

On the basis of equation (10), the law is designed as follows:

$$\dot{\boldsymbol{s}}=-\left(\frac{\lambda}{\Phi(\boldsymbol{s})}+\rho\right)\mathrm{sign}(\boldsymbol{s})-\gamma\left(1-\mathrm{e}^{-\xi|\boldsymbol{s}|}\right)\boldsymbol{s}\,(13)$$

$\Phi(\boldsymbol{s})=\varphi+\left(1+1/|\varepsilon|-\varphi\right)\cdot\mathrm{e}^{-\sigma|\boldsymbol{s}|}$ $\lambda,\gamma,\sigma,\xi>0$ $0<\varphi<1$ ρ $|\boldsymbol{s}|\to\infty$ $\Phi(\boldsymbol{s})$ φ $\lambda/\Phi(\boldsymbol{s})>\lambda$ $\gamma\left(1-\mathrm{e}^{-\xi|\boldsymbol{s}|}\right)$ γ $|\boldsymbol{s}|\to 0$ $\Phi(\boldsymbol{s})$ $1+1/|\varepsilon|$ $\lambda/\Phi(\boldsymbol{s})<\lambda$ $\lambda/\Phi(\boldsymbol{s})+\rho$ Where:;;; is a very small normal number. It can be seen that when the system state is far away from the sliding mode surface, and approaching the sliding mode surface, the system state quickly approaches the sliding mode surface, then decreases to a small value, the exponential item gain approaches to 0, and the rate of the system state approach will decrease, so as to alleviate the shaking condition.

According to the designed sliding mode surface and approach law, the controller output is:

$$\boldsymbol{u}=\boldsymbol{u}_{\mathrm{eq}}+\boldsymbol{u}_{\mathrm{n}}\,(14)$$

$\boldsymbol{u}_{\mathrm{eq}}$ Where is the equivalent control term when the system state reaches the sliding mode surface, and is a robust control term. $\boldsymbol{u}_{\mathrm{n}}$

$\boldsymbol{s}=\dot{\boldsymbol{s}}=0$ Order, and represent the unknown state in IESO, get: z_3 $\boldsymbol{x}_3$

$$\boldsymbol{u}_{\mathrm{eq}} = \boldsymbol{M}_0(\boldsymbol{q})\begin{pmatrix} \ddot{\boldsymbol{q}}_d - \boldsymbol{z}_3 - \boldsymbol{K}_1\dot{\boldsymbol{\varepsilon}} - \\ \boldsymbol{K}_2 r \mathrm{sig}^{r-1}(\boldsymbol{\varepsilon})\dot{\boldsymbol{\varepsilon}} \end{pmatrix} (15)$$

To meet the arrival conditions of sliding mode control, the following robust control items are designed: $s\dot{s} \le 0$

$$\boldsymbol{u}_{\mathrm{n}} = -\boldsymbol{M}_0(\boldsymbol{q})\begin{bmatrix} \left(\dfrac{\lambda}{\Phi(\boldsymbol{s})} + \rho\right)\mathrm{sign}(\boldsymbol{s}) + \\ \gamma\left(1 - \mathrm{e}^{-\xi|\boldsymbol{s}|}\right)\boldsymbol{s} \end{bmatrix} (16)$$

At this point, bringing formula (15) and formula (16) into formula (14) can obtain the designed sliding mode control law. $\boldsymbol{u}$

2.3 Anti-saturation Compensation Scheme Design

On the basis of IESO compensation capacity, an adjustable compensation coefficient is designed, and an anti-saturation scheme based on Output Error Compensation-base error compensation (OEC) is proposed, so that the anti-saturation performance can be adjusted according to the need. The anti-saturation scheme does not need to introduce a new compensation system and simplifies the system structure while guaranteeing the compensation capacity.

The IESO based on the output error compensation has the following form:

$$\begin{cases} \boldsymbol{\varepsilon} = \boldsymbol{z}_1 - \boldsymbol{y} \\ \dot{\boldsymbol{z}}_1 = \boldsymbol{z}_2 - \beta_{01}\boldsymbol{\varepsilon} \\ \dot{\boldsymbol{z}}_2 = \boldsymbol{z}_3 - \beta_{02}\mathrm{ifal}(\boldsymbol{\varepsilon}, \alpha_1, \mu) + b_0\boldsymbol{u} \\ \qquad - b_0\boldsymbol{K}_{\mathrm{c}}\left(\boldsymbol{u} - \mathrm{sat}(\boldsymbol{u})\right) \\ \dot{\boldsymbol{z}}_3 = -\beta_{03}\mathrm{ifal}(\boldsymbol{\varepsilon}, \alpha_2, \mu) \end{cases} (17)$$

$\boldsymbol{K}_{\mathrm{c}}$ In the tunable compensation gain coefficient matrix, the large gain can promote the faster compensation of errors, but the too large gain may cause the observer instability.

3 System stability analysis

Lemma 1[12]Suppose there is a smooth and continuous positive definite Lyapunov function, and, in the neighborhood of the origin, satisfy:, where:, and are normal numbers and. At this time, for any particular one, the finite-time stable convergence time is satisfied: $\boldsymbol{V}(x)$ $\boldsymbol{V}(0)=0$ $\boldsymbol{V}(x)$ $\boldsymbol{O}\subseteq\boldsymbol{A}\subseteq\mathbf{R}^n$ $\dot{\boldsymbol{V}}(x)+c\boldsymbol{V}^{\partial}(x)\leq 0$ $\boldsymbol{O}\rightarrow\mathbf{R}$ c ∂ $\partial\in(0,1)$ t_0 t_{r}

$$t_{\mathrm{r}}\leq\frac{\boldsymbol{V}^{1-\partial}(t_0)}{c(1-\partial)} \tag{18}$$

3.1 Convergence Analysis of IESO

Suppose that the third-order linear system obtained from the expansion of the second-order disturbance system is:

$$\begin{cases}\dot{\boldsymbol{x}}_1=\boldsymbol{x}_2\\ \dot{\boldsymbol{x}}_2=\boldsymbol{x}_3+b_0\boldsymbol{u}\\ \dot{\boldsymbol{x}}_3=\zeta(t)\\ \boldsymbol{y}=\boldsymbol{x}_1\end{cases} \tag{19}$$

When the external disturbance is zero, the following error equation can be obtained according to equations (6) and (19):

$$\begin{cases}\dot{\boldsymbol{\varepsilon}}_1=\boldsymbol{\varepsilon}_2-\beta_{01}\boldsymbol{\varepsilon}_1\\ \dot{\boldsymbol{\varepsilon}}_2=\boldsymbol{\varepsilon}_3-\beta_{02}\mathrm{ifal}(\boldsymbol{\varepsilon}_1,\alpha_1,\mu)\\ \dot{\boldsymbol{\varepsilon}}_3=-\beta_{03}\mathrm{ifal}(\boldsymbol{\varepsilon}_1,\alpha_2,\mu)\end{cases} \tag{20}$$

The above formula can be rewritten as:

$$\dot{\boldsymbol{\varepsilon}}=-\boldsymbol{G}(\boldsymbol{\varepsilon})\boldsymbol{\varepsilon} \tag{21}$$

In formula:

$$\boldsymbol{G}(\boldsymbol{\varepsilon})=\begin{bmatrix}\beta_{01} & -1 & 0\\ \beta_{02}g(\boldsymbol{\varepsilon}_1) & 0 & -1\\ \beta_{03}g(\boldsymbol{\varepsilon}_1) & 0 & 0\end{bmatrix}; \quad ; \quad \boldsymbol{\varepsilon}=[\boldsymbol{\varepsilon}_1 \quad \boldsymbol{\varepsilon}_2]^{\mathrm{T}}$$

$$g\left(\varepsilon_1\right)=\frac{\text{ifal}(\varepsilon_1,\alpha_i,\mu)}{\varepsilon_1},i=1,2$$

$g\left(\varepsilon_1\right)$ $0<g\left(\varepsilon_1\right)<\kappa_1+\kappa_2\tan\varepsilon/\varepsilon$ And it is satisfied and bounded.

Select the positive definite Lyapunov function for the system (21)[13]:

$$V_0=\int_0^t\left(\boldsymbol{HG}\left(\varepsilon\right)\boldsymbol{\varepsilon},\dot{\boldsymbol{\varepsilon}}\right)d\tau\,(22)$$

$\boldsymbol{H}$ Where the matrix is presented as follows:

$$\boldsymbol{H}=\begin{bmatrix} h_{11} & h_{12} & h_{13} \\ -h_{12} & h_{22} & h_{23} \\ -h_{13} & -h_{23} & h_{33} \end{bmatrix}(23)$$

Lemma 2[14] $\boldsymbol{H}$ $\boldsymbol{HG}(\varepsilon)$ If there is a matrix whose main diagonal element is positive, so that the matrix is positive definite and symmetric, then the zero solution of the system (21) is Lyapunov stable, and then Lyapunov is gradually stable.

$\boldsymbol{HG}(\varepsilon)$ The matrix may be expressed as follows:

$$\boldsymbol{HG}\left(\varepsilon\right)=\begin{bmatrix} H_{11} & -h_{11} & -h_{12} \\ H_{21} & h_{12} & -h_{22} \\ H_{31} & h_{13} & h_{23} \end{bmatrix}(24)$$

In formula:

$$\begin{cases} H_{11}=h_{11}\beta_{01}+h_{12}\beta_{02}g\left(\varepsilon_1\right)+h_{13}\beta_{03}g\left(\varepsilon_1\right) \\ H_{21}=-h_{12}\beta_{01}+h_{22}\beta_{02}g\left(\varepsilon_1\right)+h_{23}\beta_{03}g\left(\varepsilon_1\right) \\ H_{31}=-h_{13}\beta_{01}-h_{23}\beta_{02}g\left(\varepsilon_1\right)+h_{33}\beta_{03}g\left(\varepsilon_1\right) \end{cases}$$

$\boldsymbol{HG}(\varepsilon)$ To be positive definite and symmetric, the following conditions need to be met:

$$\begin{cases} h_{22} = -h_{13} \\ H_{31} = -h_{12} \\ H_{21} = -h_{11} \end{cases} (25)$$

$$H_{11} > 0 (26)$$

$$\begin{vmatrix} H_{11} & -h_{11} \\ -h_{11} & h_{12} \end{vmatrix} > 0 (27)$$

$$\begin{vmatrix} H_{11} & -h_{11} & -h_{12} \\ -h_{11} & h_{12} & -h_{22} \\ -h_{12} & -h_{22} & h_{23} \end{vmatrix} > 0 (28)$$

$h_{11} = 1$ $h_{22} = h_{33} = \delta$ δ Order,, is positive and infinitely close to zero. After calculation and deduction, when the conditions are met, the matrix satisfying the lemma 2 can be obtained, so that the matrix is positive definite and symmetric, and the corresponding equation (22) is satisfied: $\beta_{01}\beta_{02} - \beta_{03} > 0$ $\boldsymbol{H}$ $\boldsymbol{HG}(\boldsymbol{\varepsilon})$

$$\dot{\boldsymbol{V}}_0 = -\left(\boldsymbol{HG}(\boldsymbol{\varepsilon})\boldsymbol{\varepsilon}, \boldsymbol{G}(\boldsymbol{\varepsilon})\boldsymbol{\varepsilon}\right) < 0 (29)$$

That is, the system (21) is asymptotically stable for Lyapunov.

3.2 Stability Analysis of FNTSM Controller

Define the following Lyapunov function:

$$\boldsymbol{V}_1 = \frac{1}{2}\boldsymbol{s}^2 (30)$$

The first-order derivative is:

$$\dot{\boldsymbol{V}}_1 = \boldsymbol{s}\dot{\boldsymbol{s}} = \boldsymbol{s}\begin{pmatrix} \boldsymbol{M}_0^{-1}\boldsymbol{u} + \boldsymbol{x}_3 - \ddot{\boldsymbol{q}}_{\mathrm{d}} + \\ \boldsymbol{K}_1\dot{\boldsymbol{\varepsilon}} + \boldsymbol{K}_2 r|\boldsymbol{\varepsilon}|^{r-1}\dot{\boldsymbol{\varepsilon}} \end{pmatrix} (31)$$

Bring the formula (14) into the upper formula available:

$$\begin{aligned}\dot{V}_1 &= s\left[-\left(\frac{\lambda}{\Phi(s)}+\rho\right)\operatorname{sign}(s)-\gamma\left(1-e^{-\xi|s|}\right)s\right] \\ &= -\left(\frac{\lambda}{\Phi(s)}+\rho\right)|s|-\gamma\left(1-e^{-\xi|s|}\right)s^2 \qquad (32) \\ &\le -\left(\frac{\lambda}{\Phi(s)}+\rho\right)|s| \le -\rho|s|\end{aligned}$$

ρ Since it is a very small normal number, it holds, satisfying the Lyapunov stability condition. $\dot{V}_1 \le 0$ The combinations of formula (30) and formula (32) are available:

$$\dot{V}_1 \le -\sqrt{2}\rho V_1^{1/2} \text{ (33)}$$

By lemma 1, the system can converge at a finite time. $t_r \le \frac{\sqrt{2}}{\rho} V_1^{1/2}(0)$

In summary, the positive definite function of the whole control system is defined as $V = V_0 + V_1$ $\dot{V} = \dot{V}_0 + \dot{V}_1 < 0$, From Equations (40) and (43), the system is asymptotically stable according to the Lyapunov stability criterion. The system tracking error will converge to a small neighborhood along the sliding surface to zero in finite time. t_r

4 Simulation analysis and validation

In order to verify the effectiveness and accuracy of the proposed method under the external interference and nonlinear influence of dead area, the design simulation test of the joint track tracking control system with the help of MATLAB / Simulink software. Taking the 2-DOF robotic arm as an example, the model parameters of the kinetic equation (1) are as follows:

$$\begin{cases} \boldsymbol{M}(\boldsymbol{q}) = \begin{bmatrix} m_{11} & m_{12} \\ m_{21} & m_{22} \end{bmatrix} \\ \boldsymbol{C}(\boldsymbol{q},\dot{\boldsymbol{q}}) = \begin{bmatrix} -C \cdot \dot{q}_2 & -C \cdot (\dot{q}_1 + \dot{q}_2) \\ C \cdot \dot{q}_1 & 0 \end{bmatrix} \\ \boldsymbol{G}(\boldsymbol{q}) = \begin{bmatrix} G_1 + G_2 \\ G_2 \end{bmatrix} \end{cases} (34)$$

In formula:

$$\begin{aligned} &m_{11} = (m_1 + m_2) l_1^2 + m_2 l_2^2 + 2 m_2 l_1 l_2 \cos(q_2) \\ &m_{12} = m_{21} = m_2 l_2^2 + m_2 l_1 l_2 \cos(q_2) \\ &m_{22} = m_2 l_2^2 \\ &C = m_2 l_1 l_2 \sin(q_2) \\ &G_1 = (m_1 + m_2) l_1 g \cos(q_2) \\ &G_2 = m_2 l_2 g \cos(q_1 + q_2) \end{aligned}$$

The physical parameters of the 2-DOF manipulator are shown in Table 1, and the values of the controller parameters are shown in Table 2. Considering the error in the actual system model dynamics, the system uncertainty is set to 10% of the system nominal value, i. e

$$\begin{cases} \eta \boldsymbol{M}(\boldsymbol{q}) = 0.1 \boldsymbol{M}_0(\boldsymbol{q}) \\ \eta \boldsymbol{C}(\boldsymbol{q},\dot{\boldsymbol{q}}) = 0.1 \boldsymbol{C}_0(\boldsymbol{q},\dot{\boldsymbol{q}}) \\ \eta \boldsymbol{G}(\boldsymbol{q}) = 0.1 \boldsymbol{G}_0(\boldsymbol{q}) \end{cases} (35)$$

$\boldsymbol{q}(0) = [0.5 \ 0.3]^{\mathrm{T}}$ $\dot{\boldsymbol{q}}(0) = [0 \ 0]^{\mathrm{T}}$ Let the system initial position state rad, the initial velocity state rad / s, and the reference expectation signal is set to. $\boldsymbol{q}_{\mathrm{d}} = [2\sin(t) + \sin(0.5t) \quad \cos(t) + \cos(0.5t)]^{\mathrm{T}}$

Table 1 2-Physical parameters of the DOF robotic arm

symbol	definition	numeric value
m_1	Link 1 mass	2.1 kg

m_2	Link 2 mass	.6 2kg
l_1	Link 1 length	0.26 m
l_2	Link 2 length	0.24 m
g	gravitational constant	9.81 m/s^2

Table 2 Controller parameters

symbol	numeric value	symbol	numeric value
r	$5/3$	ρ	0.001
K_1	$\mathrm{diag}(60,60)$	β_{01}	120
K_2	$\mathrm{diag}(30,30)$	β_{02}	1500
λ	2	β_{03}	12000
φ	0.5	α_1	0.5
σ	1	α_2	0.25
ξ	1.5	μ	0.02
γ	80	$\boldsymbol{K}_c$	$\mathrm{diag}(0.6,1.2)$

To verify the robustness of this method, friction force and external time-varying disturbance signals are considered in the system: $\boldsymbol{f} = 0.3\mathrm{sign}(\dot{\boldsymbol{q}}) + 0.5\dot{\boldsymbol{q}}$ $\boldsymbol{\tau}_{\mathrm{d}}$

$$\begin{cases} \boldsymbol{\tau}_{\mathrm{d}} = \begin{bmatrix} 0 \\ 0 \end{bmatrix} & t < 10 \\ \boldsymbol{\tau}_{\mathrm{d}} = \begin{bmatrix} 10\sin(2t) + 5\cos(1.5t) \\ 5\cos(1.5t) + 2.5\sin(0.5t) \end{bmatrix} & t \geq 10 \end{cases}$$

Figure 2 to Figure 4 show the simulation results of the saturation compensation (OEC-ISFAC) method and the unsaturation compensation (ISFAC), the saturation compensation scheme (SC-ISFAC) and the traditional self-disturbance control (IS-ADRC), and the trajectory tracking effect, tracking error, error performance index and control input signal curve, respectively.

To quantify the analytical control performance, the integration of the absolute value of the error (IAE) and two performance indicators of its times time (ITAE) are introduced:

$$\begin{cases} \mathrm{IAE} = \int_0^{t_f} |\varepsilon(t)| dt \\ \mathrm{ITAE} = \int_0^{t_f} t|\varepsilon(t)| dt \end{cases} \quad (36)$$

t_fWhere, it is the system run time. See Figure 3 for the specific indicators.

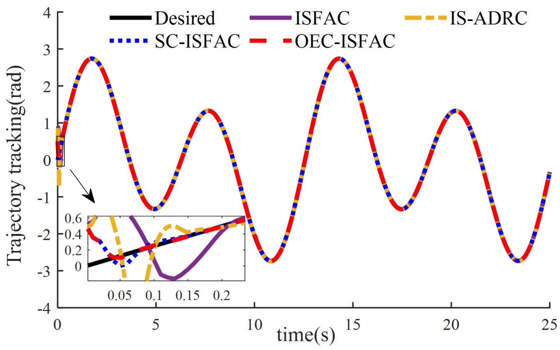

(a)Joint 1

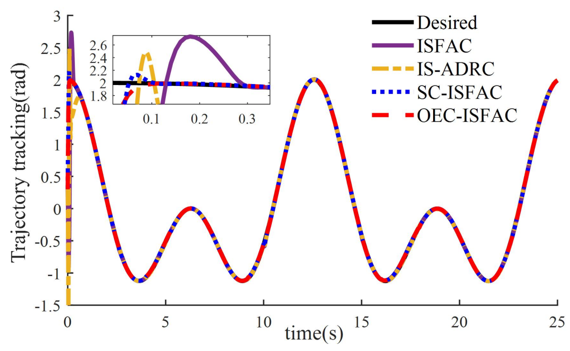

(b)Joint 2

Fig 2 Joint trajectory tracking effect curve s

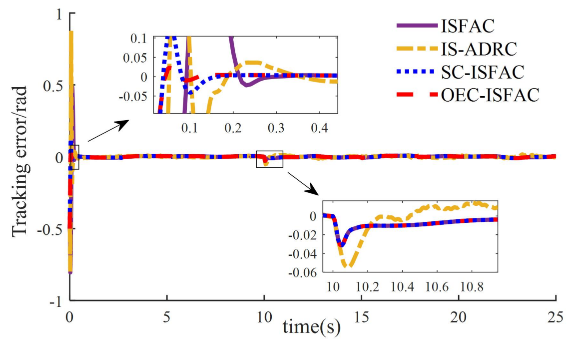

(a)Joint 1

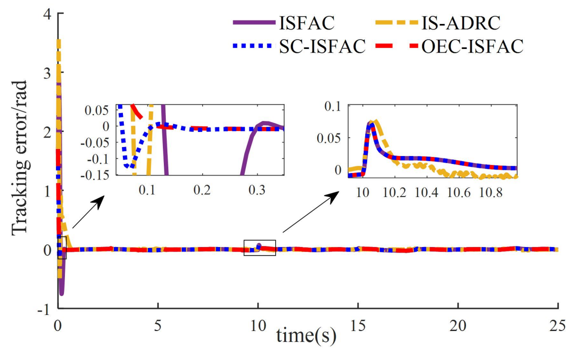

(b)Joint 2

Fig 3 Joint trajectory tracking error curve s

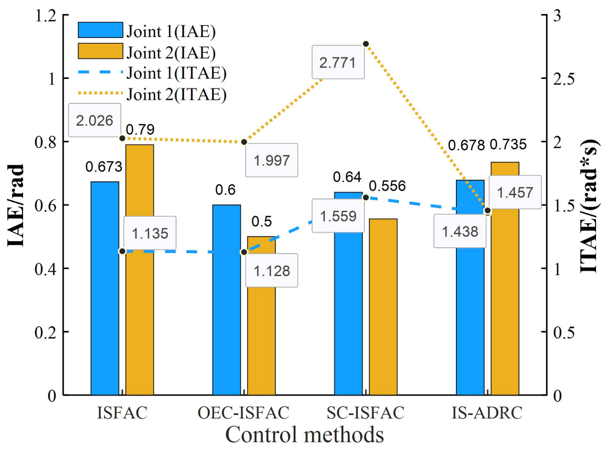

Fig 4 Performance indices

As can be seen from Figure 2 to and Figure 4, the present method shows better error performance, with high tracking curve fit of joint 1 and joint 2, and the tracking error converges at about 0.15s. After 10s of external interference, the proposed method can return the error curve to steady state in a shorter time. Although the SC-ISFAC method also shows the ideal saturation compensation effect and control accuracy, the convergence rate is worse than the proposed method, and it needs to introduce the compensation system, which increases the complexity of the control system.

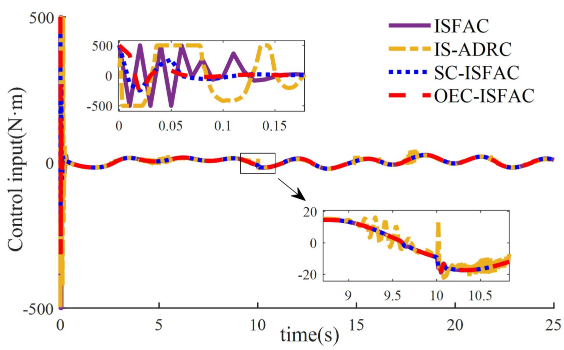

(a)Joint 1

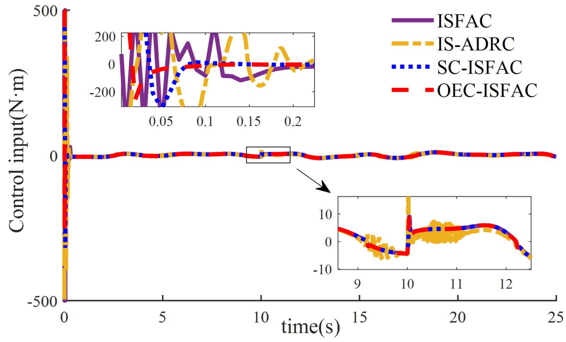

(b)Joint 2

Fig 5 Joint control input response curve s

Figure 5 shows the joint control input curve with a saturation limit of ±500 Nm, combining Figure 2 and Figure 3, without the anti-saturation compensation scheme, the control input curve showed obvious fluctuation during the initial operation of the mechanical arm, because the actuator saturation affects the stability of the system operation and causes the system to use the original torque without compensating the missing torque, which leads to the control performance delay and slow tracking and error convergence rate. Although IS-ADRC shows similar error performance to ISFAC, its control input has obvious vibration and poor control stability.

From the simulation results, under the proposed method, due to the design of OEC saturation scheme, the system control performance, showing better error performance and higher control accuracy, and the control input curve after about 0.1s rapid convergence, into the steady state is stable in about ±20 Nm and ±10 Nm interval, and the torque curve under the proposed method is more smooth and stable, can ensure the smooth operation of the system.

Considering that the deviation of each joint trajectory during the operation of the mechanical arm will be further amplified to the end position, the following end trajectory tracking simulation verification is conducted. Figure 6 shows the terminal trajectory tracking curve in the workspace corresponding to the joint motion under the proposed method. Where the initial position is, Figure 6 (a) is the end position curve, and Figure 6 (b) is the position tracking error curve of each axis at the end. $(x_0, y_0, z_0) = (0.38, 0.33, -0.07)$

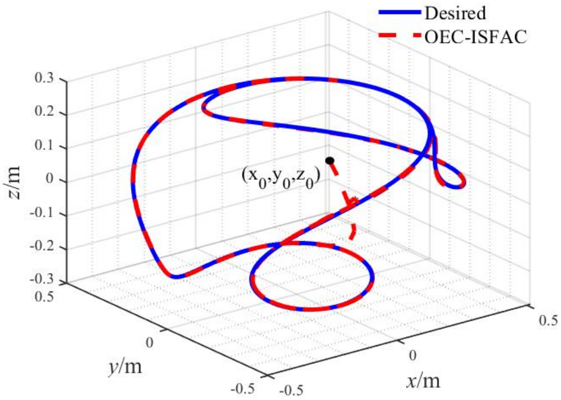

(a) T erminal position

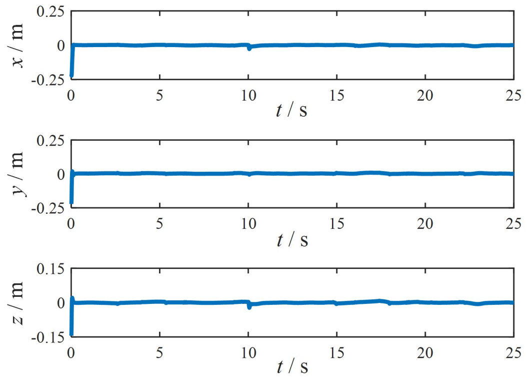

(b) End axis tracking error

Fig 6 End effector trace curve s

As can be seen from figure 6, under the proposed method, the terminal position curve showed ideal fit, and the end of the position of the axis can converge in a short time, and show small steady state error, further reflects the joint track tracking only showed little deviation, prove that the proposed algorithm can achieve the ideal track tracking effect.

5 Conclusion

Under the influence of the compound disturbance, Mechanical arm system with nonlinear characteristics of input saturation and dead zone, Using the ADRC as the framework, A modified ESO estimation is designed and compensates for the total system disturbance; Combined with FNTSM and variable gain sliding mode approach law, An improved slip-mode self-immunity algorithm was designed, The fast and high-precision joint track tracking and control of the robotic arm system in a limited time is realized; Regarding the reduction of control accuracy and stability of the system caused by actuator saturation, Design of an anti-saturation scheme based on the output error compensation, Effective compensation is realized; Based on the Lyapunov-stability theory, The stability of the control system is verified. The simulation results show that the proposed method has strong stability and effectively improves the control accuracy and response speed.

References

[1] DONG M, SUN G H, et al. Impedance control of multi-arm space robot for the capture of non- cooperative targets[J] Journal of Systems Engineering and Electronics, 2020, 31(5): 1051-1061.

[2] SON J, KANG H, KANG S H. A review on robust control of robot manipulators for future manufacturing[J]. International Journal of

Precision Engineering and Manufacturing, 2023, 24(6): 1083-1102.

[3] SAI H, XU Z, HE S, et al. Adaptive nonsingular fixed-time sliding mode control for uncertain robotic manipulators under actuator saturation [J]. ISA transactions, 2022, 123: 46-60.

[4] SUN Y, KUANG J, GAO Y, et al. Fixed-time prescribed performance tracking control for manipulators against input saturation[J]. Nonlinear Dynamics, 2023, 111(15): 14077-14095.

[5] SPONG M W. An historical perspective on the control of robotic manipulators[J]. Annual Review of Control, Robotics, and Autonomous Systems, 2022, 5: 1-31.

[6] Huang Chenjing, Zhang Lei, Sun Xun et al. Trajectory tracking Control Method of fabric Grasping Manipulator Based on Dynamic Model [J]. Acta Textile Sinica,2023, 44(06): 207-214.(in Chinese)

[7] WEI H, JIANG Y. Adaptive fast nonsingular terminal sliding mode tracking control for quadrotor with disturbances compensation and actuator saturation[J]. Proceedings of the Institution of Mechanical Engineers, Part C: Journal of Mechanical Engineering Science, 2024, 238(2): 301-319.

[8] Chen Zhengsheng, Wang Xuesong, Cheng Yuhu. Continuous non-singular fast terminal sliding Mode Control of Manipulator considering disturbance and input saturation [J]. Control and

Decision, 2012,37(04): 903-912.(in Chinese)

[9] Zhang Lei, Song Boxiong, Tian Dongyu. Trajectory tracking sliding mode control of manipulator considering input saturation [J]. Journal of Xi 'an Polytechnic University, 2024, 38(02): 85-92.(in Chinese)

[10] FENG Y, YU X H, MAN Z H. Non-singular terminal sliding mode control of rigid manipulators[J].Automatica,2002,38(12):2159-2167.

[11] Han Jingqing. Active Disturbance Rejection Controller and Its Application [J]. Control and Decision, 1998(01):19-23.(in Chinese)

[12] BHAT S, BERNSTEIN D S. Lyapunov analysis of finite-time differential equations[C]// Proceedings of 1995 American Control Conference, WA, USA, 1995, 3:1831-1832.

[13] LOZGACHEV G I. On a method of construction of Lyapunov functions[J]. Automation and Remote Control, 1998, 59 (10):1365-1368.

[14] Gan Zuoxin, Han Jingqing. Lyapunov Function Construction of second-order ESO [C]// Control Theory Committee of the Chinese Society of Automation, Proceedings of the 21st Chinese Control Conference, Zhejiang University Press, 2002:365-368.(in Chinese)